Environ Sci Pollut Res (2015) 22:16721–16731
DOI 10.1007/s11356-015-4866-z

RESEARCH ARTICLE

Isotherm, kinetic, and thermodynamic studies on Hg(II) adsorption from aqueous solution by silica- multiwall carbon nanotubes

Tawfik A. Saleh [1]

Received: 8 April 2015 / Accepted: 8 June 2015 / Published online: 20 June 2015

Abstract Silica combined with 2 % multiwall carbon nanotubes (SiO_2-CNT) was synthesized and characterized. Its sorption efficacy was investigated for the Hg(II) removal from an aqueous solution. The effect of pH on the percentage removal by the prepared material was examined in the range from 3 to 7. The adsorption kinetics were well fitted by using a pseudo-second-order model at various initial Hg(II) concentrations with R^2 of >0.99. The experimental data were plotted using the interparticle diffusion model, which indicated that the interparticle diffusion is not the only rate-limiting step. The data is well described by the Freundlich isotherm equation. The activation energy (Ea) for adsorption was 12.7 kJ mol^{-1}, indicating the process is to be physisorption. Consistent with an endothermic process, an increase in the temperature resulted in increasing mercury removal with a ΔH^o of 13.3 kJ/mol and a ΔS^o 67.5 J/mol K. The experimental results demonstrate that the combining of silica and nanotubes is a promising alternative material, which can be used to remove the mercury from wastewaters.

Keywords SiO_2-CNT · Environmental degradation · Surface analysis

Responsible editor: Philippe Garrigues

✉ Tawfik A. Saleh
tawfik@kfupm.edu.sa; tawfikas@hotmail.com; http://faculty.kfupm.edu.sa/CHEM/tawfik/publications.html

[1] Chemistry Department, King Fahd University of Petroleum & Minerals, Dhahran 31261, Saudi Arabia

Introduction

Nowadays, in an industrial world, one of the most important concerns is securing the health of the human race and the environment. Toxic pollutants are released into the environment as a result of industrial activities. Mercury (Hg), as a toxic pollutant, is distributed in the environment (Wang et al. 2012). In addition to natural sources, human production and industrial activities such as pulp, paper, plastic industry, oil refining, cement production, and household waste are sources of pollution (Fu et al. 2012). Methods of coagulation, filtration, precipitation, ozonation, ion exchange, etc. have been reported. However, adsorption is considered a more attractive process because of its simple design. Locally available materials such as natural materials and agricultural forget and industrial wastes can be utilized as low-cost adsorbents.

Various conventional adsorbents such as carbon materials, carbons derived from agricultural wastes and industrial wastes, biomaterials, and other materials have been investigated for the mercury removal (Yardim et al. 2003; Labidi 2008; Anirudhan et al. 2008; Sari and Tuzen, 2009; Mehdinia et al. 2015; Vasudevan et al. 2012; Wang et al. 2014) but they are not highly efficient. Therefore, researchers are still making great efforts to identify new adsorbents with high capacities and efficacies. Nowadays, the applicability of nanomaterials in pollutant removal has become a focus because of their good absorption properties (Zhang et al. 2013). Hybrid ligand-modified activated carbon, modified activated carbon, carbon nanotubes, and composite beads (Zhu et al. 2009; Shawky et al. 2012; Shadbad et al. 2011) have also been studied for the mercury removal.

The unique structural, chemical, physical, and mechanical properties of multiwall carbon nanotubes discovered by Iijima (Iijima 1991) have led more research to various interdisciplinary investigations (Saleh and Gupta 2014). Among inorganic materials, silica has aroused great interest due to its mechanical properties and structural features, for instance, facile surface functionalization, easy incorporation with other materials, high surface area, and pore volume (Insin et al. 2008).

Various methods, such as the traditional templating and interfacial growth, have been reported for the synthesis of silica nanotubes, mesoporous silica nanoparticle, nanoparticles loaded silica microspheres, and monodispersed mesoporous silica (Insin et al. 2008; Kim et al. 2011; Zhang et al. 2010).

However, the combining of the properties of silica and CNTs into a composite and its sorption potential have not been studied extensively. In this work, the sorption performance of silica was enhanced by introducing CNT. The SiO_2-CNT was prepared and its sorption efficiency was evaluated for the Hg(II) removal from waters. Various experimental parameters were optimized and isotherms and kinetics models were fitted to the results.

Materials and methods

Chemicals and materials

The multiwall carbon nanotubes were purchased from Cheap Tubes Com. The standard stock mercury solution (1000 mg/l) Hg(II) was used. The initial pH of the tested solutions was adjusted by nitric acid or sodium hydroxide.

Synthesis of SiO_2-CNT

The raw nanotubes were treated with concentrated sulphuric and nitric acids as per the method reported earlier (Saleh 2011). For the synthesis of non-calcined SiO_2-CNT, oxidized nanotubes were dispersed in 0.1 L deionized water and 0.05 L ethylene glycol under stirring for 5 h. Sodium meta-silicate (0.5 mol/L) was introduced into the dispersed nanotubes under stirring. The ammonia was used to adjust the pH at 9, followed by reflux at 120 °C for 12 h. After cooling, it was carefully filtered and rinsed with water. After that, it was dried at 100 °C and, then, used as an adsorbent without calcination.

Characterization

Several techniques were employed to characterize the SiO_2-CNT. A scanning electron microscope was employed for morphology characterization. Energy-dispersive X-ray spectroscope (EDX) was used for elemental analysis of the samples. To determine the composition and crystalline structure of the prepared material, X-ray diffraction (XRD) pattern was obtained by a powder X-ray diffraction (Quantachrome, NOVA2000) using Cu-kα radiation, λ=1.54 Å at 25 °C.

A Thermo Electron Corporation NXR FT-Raman module Nicolet 6700 FT-IR spectrometer in a region of 4000–400 cm^{-1} was used for IR characterization of the SiO_2-CNT. Thermal analysis was conducted to determine the thermal stability using a thermal analyzer (STA 429) (Netzsch, Germany) at a constant heating rate of 10 °C/min under nitrogen flow.

Hg(II) determination was carried out with the Mercury Analyzer. The real wastewater samples were monitored by inductively coupled plasma (ICP).

Point of net zero charge (pH_{zpc}) determination

Point of net zero charge (pH_{zpc}) specifies the electrical neutrality of the adsorbent at a particular value of pH under aqueous solution conditions. When a material is placed in solutions with pH higher than its PZC, the net surface charge turns negative by deprotonation, and thus adsorbs cations.

The method followed to determine the PZC of the SiO_2-CNT comprised of the following steps (Saleh and Gupta 2011). Dilute aqueous solutions were prepared to make 11 solutions with pH values of 1.0 to 12.0. A 20 ml mercury solution was placed in vials and allowed to equilibrate. Then, the initial pH of each solution was measured, and 25.0 mg of the prepared SiO_2-CNT were added to each. Flasks were capped and placed on a shaker for 24 h and then filtered. After filtration, the final pH of the filtrates was determined. The graph of pH_{intial} vs. pH_{final} was plotted and the intersection of the curve with the straight line with the slope of 45° is identified as the pH_{zpc}. This value was obtained as 4 for the reported SiO_2-CNT. It is worth mentioning that pH variation caused by protonation and/or deprotonation of an adsorbent proves the presence of functional groups. This indicates that the adsorbent acquires a negative charge in solutions of pH >4.

Adsorption tests

The experiments for batch tests were performed by adding a specific quantity of the SiO_2-CNT to pH-controlled distilled water. Thereafter, standard aliquots of the mercury stock solutions were introduced, giving resultant mercury concentrations of a range from 20 to 80 ppm. The mixtures were then mechanically agitated to promote adsorption over a 120 min period to reach the equilibrium time. After adsorption, aliquots were filtered and analyzed for mercury concentrations.

Adsorption capacity and percentage were evaluated using the equations:

$$q_e = (C_o - C_e) \times \frac{V}{m} \quad (1)$$

$$q_t = (C_o - C_t) \times \frac{V}{m} \quad (2)$$

$$\%Removal = \frac{C_o - C_e}{C_o} \times 100 \quad (3)$$

where q_e, mg/g and q_t, mg/g are the amounts of mercury adsorbed per gram of sorbent at equilibrium and t time; C_0 and C_e, mg/L, are the initial concentrations, and equilibrium liquid phase concentrations. m is the adsorbent mass in g. V is the volume in L.

Reuse of the SiO_2-CNT

The Hg-loaded SiO_2-CNT were eluted by stirring with HNO_3 (1 M) at room temperature for 3 h to desorb Hg(II). Thereafter, the SiO_2-CNT was washed and allowed to dry and then again reused in adsorption processes. The adsorption and desorption procedures were repeated five times, each time with fresh mercury solutions.

Results and discussion

Characterization

The morphology of SiO_2-CNT was investigated by SEM and EDX. The SEM image of SiO_2-CNT is depicted in Fig. 1a, which shows the nodes of silica nanoparticles on the nanotube surface. EDX was used to check the type of elements (C, O, and Si) in the sample, as depicted in Fig. 1b. TGA of the SiO_2-CNT showed two weight losses (Fig. 2). The first weight loss occurred at low temperature due to decomposition of water moisture on the nanotube surface. The second weight loss, which occurs at about 600 °C, corresponds to the CNTs oxidation. Comparing TGA of the SiO_2-CNT with that of CNTs, the thermal stability of SiO_2-CNT by silica has much improved (Zhang et al. 2010; Yin et al. 2010). Figure 3 shows XRD patterns of the SiO_2-CNT. The broadening of the diffraction peak centered at about 23° may confirm the formation of silica on the nanotubes.

Figure 4 depicts the FT-IR spectrum of the acid-treated MWCNTs (Saleh 2011). The band at 1710 cm^{-1} is attributed to the stretching modes of –COOH on the nanotube surface. The band at 1580 cm^{-1} corresponds to stretching vibrations of the C=C bonds. The broad band at 3450 cm^{-1} can be attributed to the –OH groups. For the FT-IR spectrum of SiO_2-CNT (Fig. 4), the band at 1095 cm^{-1} is attributed to the characteristic absorption peaks of Si–O vibration. The band at around 700 cm^{-1} is assigned to Si-O-Si bonds (Saikia and Parthasarathy 2010; Yin et al. 2010). Si-OH groups on silica are expected to show a sharp band at 3750–3450 cm^{-1}. Free silanol groups Si-OH show absorption in the range 810–950 cm^{-1} (Anderson 1974). The intensity of the peaks 1580 and 1720 cm^{-1} can be observed, which indicates a possible interaction between the SiO_2 and CNT (El-Gamel et al. 2011).

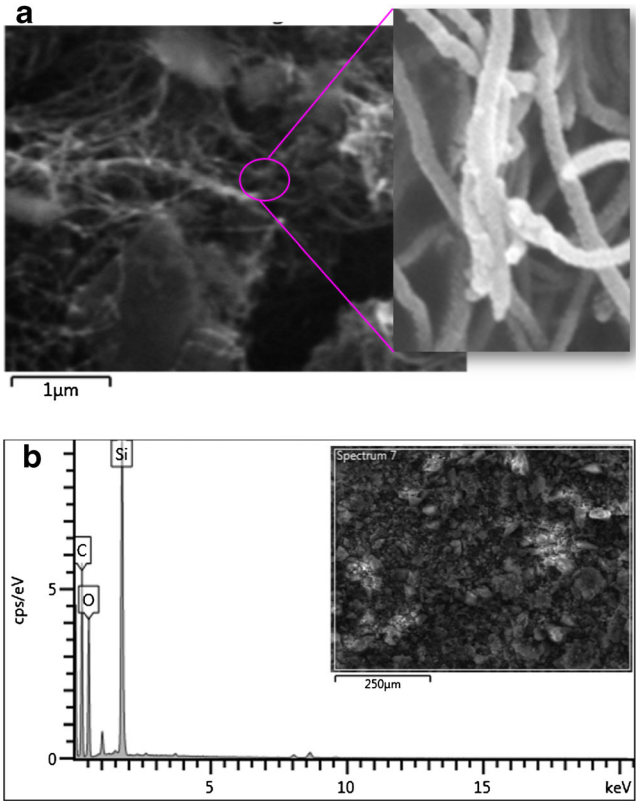

Fig. 1 FESEM image, HR-SEM image (**a**) and EDX spectrum (**b**) of the SiO_2-CNT

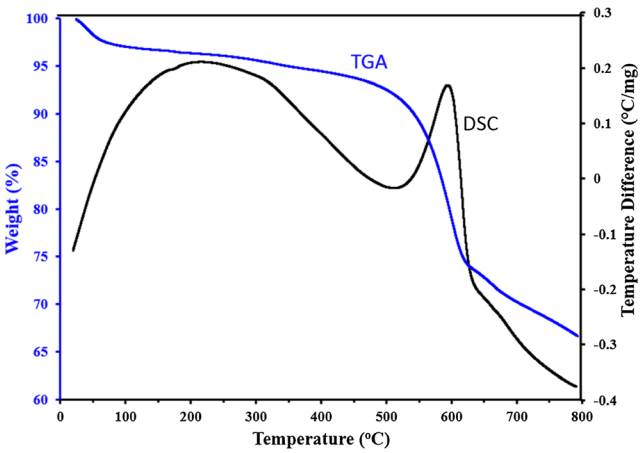

Fig. 2 TGA-DSC analysis of SiO_2-CNT

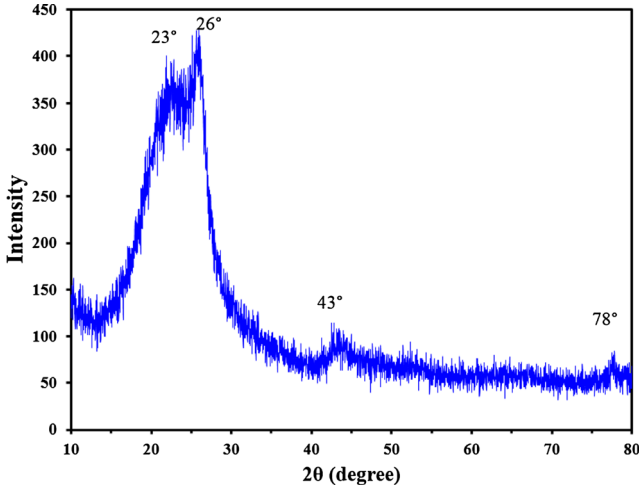

Fig. 3 XRD pattern of SiO_2-CNT

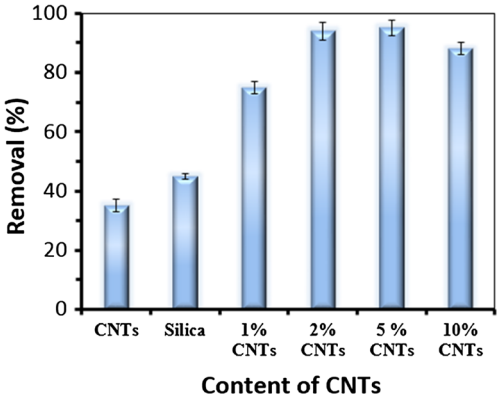

Fig. 5 Adsorption of Hg(II) by different adsorbents, with initial concentration of 40 ppm, dosage used 0.03 g, shaker agitation speed of 150 rpm, pH adjusted at 6, and contact time of 2 h

Sorption evaluation

Comparison

In order to optimize the amount of CNTs mixed with silica, a comparison study was conducted by changing the CNTs to SiO_2 ratio in the SiO_2-CNT. As depicted in Fig. 5, the amount of Hg(II) adsorbed was influenced by the ratio of CNTs to SiO_2. The optimum adsorption was obtained on SiO_2-CNT with 2–5 % of CNTs. For a comparison in adsorption, a physical mixture of silica and CNT at the same ration, 2 %, was used as an adsorbent, which showed the adsorption efficiency of approximately 53 %. Therefore, the SiO_2-CNT with 2 % CNTs was selected for this work.

Effect of operating parameters

The pH of the solution plays a dominant role in determining the sorption removal efficiency. The effect of the pH solution on the mercury adsorption was investigated (Fig. 6a). Maximum sorption efficiency was observed between pH 5 and 6. To identify the adsorption mechanism, the distribution diagram of mercury species was considered (Zhanga et al. 2005). The dominant species at pH less than 3.0 is Hg(II), and at pH ≥6 are $Hg(OH)_2$. In addition, $HgOH^+$ was also reported in a solution of pH of 2 to 6. The pH_{zpc} of the SiO_2-CNT was 4. Therefore, the surface of the SiO_2-CNT is positive in a solution of pH less than 4, because of the protonation. Hence, repulsion between Hg (II) and the adsorbent is expected, which explains the low adsorption at pH less than 4. The surface

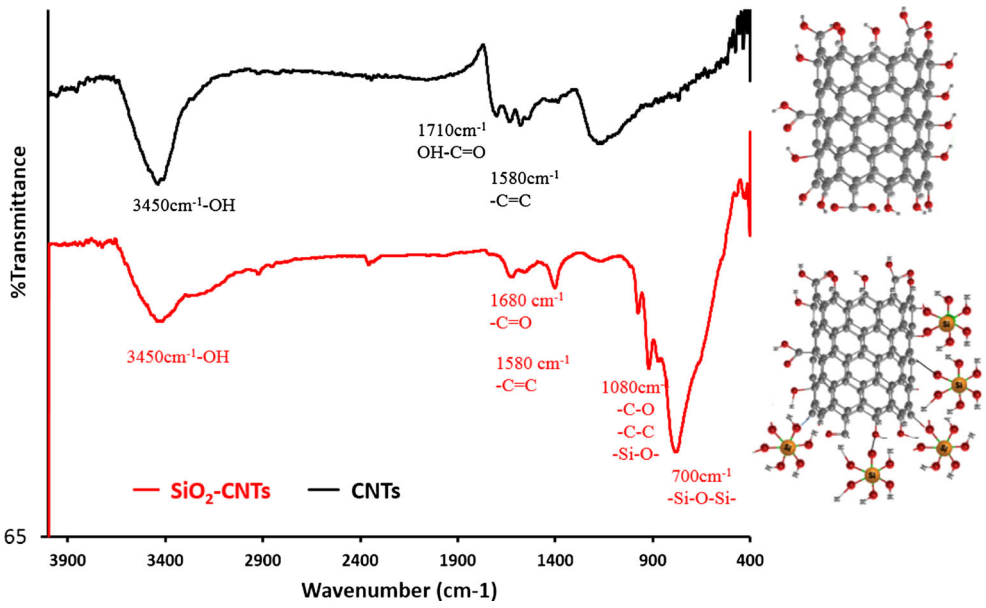

Fig. 4 FT-IR spectrum of CNTs and SiO_2-CNT

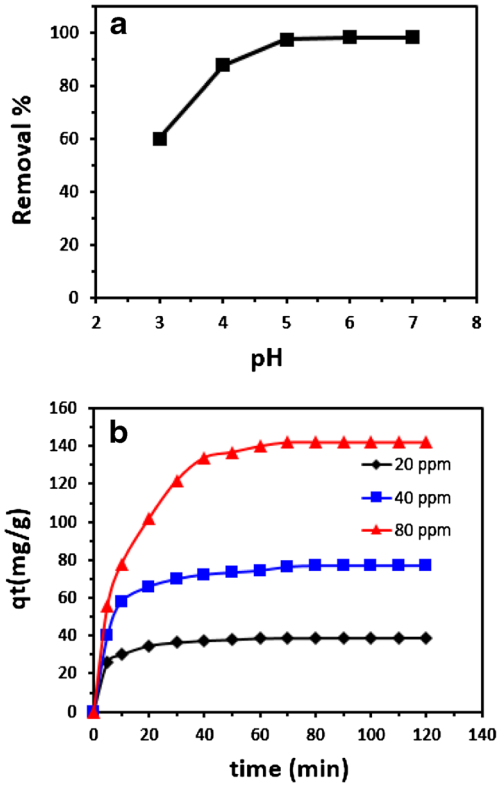

Fig. 6 Effect of pH (**a**) and contact time (**b**) on the Hg(II) adsorption on SiO_2-CNT; at room temperature ≈ 23 °C

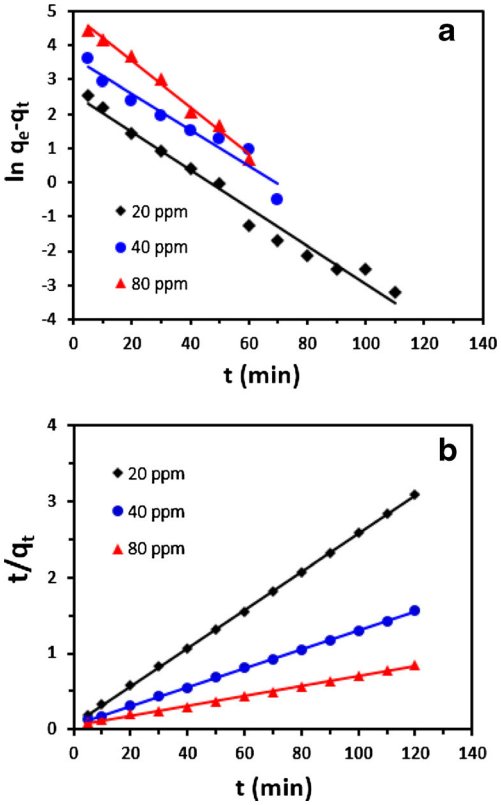

Fig. 7 Kinetics **a** Lagergren's pseudo-first; **b** pseudo-second-order; plots for Hg(II) adsorption on the surface of SiO_2-CNT, for different initial feed concentration at pH 6, 22 °C and shaker agitation speed of 150 rpm

of SiO_2-CNT is negative in a medium of pH >4 due to deprotonation, which facilitates the adsorption.

In batch experimental mode, the effect of contact time was monitored for various initial mercury concentrations (20, 40, and 80 ppm) (Fig. 6b). There was a relatively rapid initial adsorption rate of mercury at the beginning until 40 min of contact time. This could be due to the availability of all sites on the SiO_2-CNT surface and the high mercury concentration gradient. From 40 to 120 min, the rate became constant reaching the equilibrium.

Kinetic studies

The kinetic experimental results were conducted at 20, 40, and 80 ppm and analyzed to predict the adsorption constant rate using Lagergren's pseudo-first-order equation (Lagergren 1898):

$$\ln(q_e - q_t) = \ln q_e - k_1 t \tag{4}$$

the Hg(II) (mg/g) adsorbed at any time t or equilibrium are q_t or q_e. The plots of the data in Fig. 7a indicate that the adsorption process was not following the pseudo-first-order kinetic model, Table 1. Therefore, the data were modeled using the pseudo-second-order kinetic equation

$$\frac{t}{q_t} = \frac{1}{k_2 q_e^2} + \frac{t}{q_e} \tag{5}$$

k_2 in g/mg min is the pseudo-second-order rate, and q_e and q_t are the capacity. The plot of t/q_t versus t (Fig. 7b) and the values of rate parameters were summarized in Table 1. $h = k_2 q_e^2$ in mg/g min is considered the initial adsorption rate. The correlation of $q_{e,\,cal}$ with $q_{e,\,exp}$ and correlation coefficients of $R^2 > 0.99$ reveal the mechanism of adsorption was a pseudo-second-order reaction.

The intraparticle diffusion model

This model assumes that an internal diffusion process controls the adsorption capacity of the adsorbents. The particle mass balance yields the adsorption rate equation for the reactant component, which can be expressed (Webber and Chakravarti, 1974) as:

$$q_t = k_{id} t^{1/2} + C \tag{6}$$

where the rate constant of intraparticle diffusion (mg/g $min^{1/2}$) is represented as k_{id}, and the intercept (mg/g)=C.

The fitting of the experimental results to this model by plotting q_t versus $t^{1/2}$ yields three linear portions of adsorption stages. The first one is an external mass transfer at the initial time. The second one is an intraparticle diffusion of Hg(II) followed by adsorption on adsorbent interior sites. Out of the second linear portion, the slope

Table 1 Kinetic constant parameters obtained for adsorption of Hg(II)

C_i (mg/L)	q_e, exp (mg/g)	Lagergren's pseudo-first order			Pseudo-second order			Intraparticle diffusion		
		k_1 (min^{-1})	q_e, cal (mg/g)	R^2	k_2 [a]	q_e, cal (mg/g)	R^2	k_{id} [b]	C (mg/g)	R^2
20	38.88	0.0557	13.3	0.981	0.0091	39.9	0.995	1.68	7.99	0.994
40	77.01	0.0526	38.1	0.942	0.0029	79.8	0.999	1.23	12.26	0.979
80	142.00	0.0526	126.0	0.996	0.0007	163.9	0.999	1.10	19.85	0.993

[a] (g/mg min)

[b] (mg/g min)

gives the values of the diffusion constant, which are listed in Table 1. The results indicated that intraparticle diffusion is not the only rate-limiting step. Comparison of adsorption capacities from q_m of the current adsorbent for the removal of Hg(II) with some reported adsorbents is displayed in Table 2.

Adsorption isotherms

There are a number of models that have been reported which explain the mechanism by which the adsorbate is adsorbed by the adsorbent.

The Langmuir isotherm model postulates a monolayer adsorption taking place at binding sites with no interactions between the molecules adsorbed nor is transmigration on the surface of adsorbent (Langmuir, 1918). The model linear equation is:

$$\frac{C_e}{q_e} = \frac{1}{k_L q_m} + \frac{C_e}{q_m} \tag{7}$$

k_L (liters/milligrams) is the Langmuir equilibrium constant, considered as the apparent energy of adsorption. From a plot of C_e/q_e against C_e (Fig. 8a), the isotherm parameters were listed in Table 3. The low value of R^2 (<0.99) is an indication that the adsorption is not a monolayer process.

The separation factor as a characteristic parameter of this isotherm, R_L, is expressed as:

$$R_L = \frac{1}{1 + K_L C_o} \tag{8}$$

The calculated R_L (Table 3) was less than 1 indicating favorable adsorption.

The Freundlich Isotherm model is a relation between the concentrations of the targeted solute on the used adsorbent to the concentrations of the solute in the liquid. It describes the characteristics of the adsorption for the heterogeneous surface (Freundlich, 1906) using the empirical equation:

$$q_e = K_f C_e^{\frac{1}{n}} \tag{9}$$

where k_F (mg/g) = model constant or adsorption capacity, n = adsorption intensity, C_e = concentration at equilibrium (mg/L), and q_e in mg/g. The linearized equation is:

$$\ln q_e = \ln K_f + \frac{1}{n} \ln C_e \tag{10}$$

From linear plot Ln q_e versus Ln C_e (Fig. 8b), the parameters were shown in Table 3. If the value of 1/n is less than one, it indicates a normal adsorption, while 1/n being >1 indicates cooperative adsorption. $1 > n < 10$

Table 2 Comparison of the adsorption capacity obtained experimentally of the reported SiO_2-CNT and adsorbents reported in the literature for Hg(II)

Sorbent materials	Adsorption capacity q_m (mg/g)	Ref
3-mercaptopropyl-trimethoxysilane (MPTMS)	27.7 67.6	Yu et al. 2012
Polyaniline/attapulgite	800	Cui et al. 2012
Carbon aerogel	34.96	Kadirvelu et al. 2008
Waste rubber	4.0	Knocke and Hemphill 1981
Activated carbon made from Sago waste	55.6	Kadirvelu et al. 2004
Malt spent rootless	50	Saifuddin and Raziah 2007
SiO_2-CNT	163.9	This work

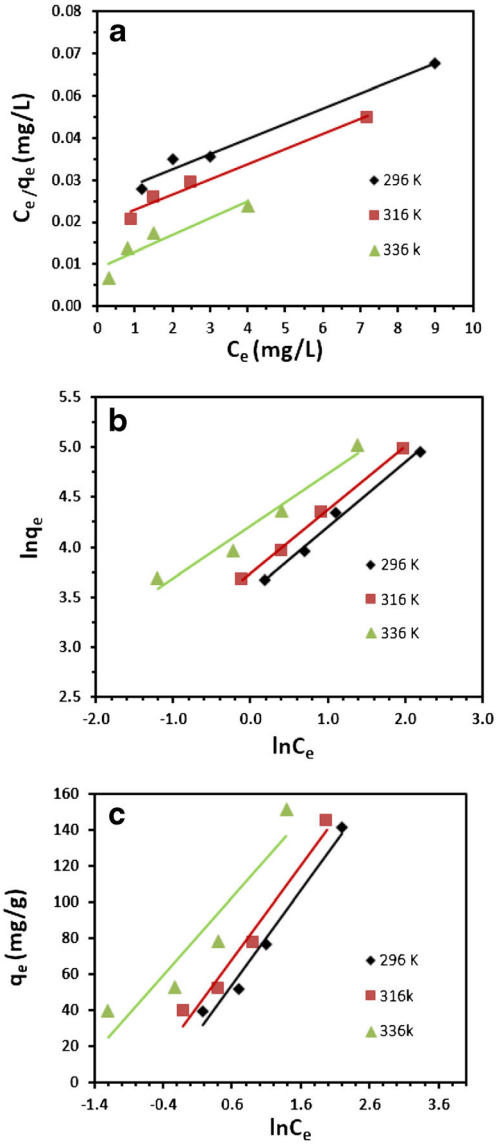

Fig. 8 Langmuir (**a**), Freundlich (**b**), and Temkin (**c**) adsorption isotherms for Hg(II) adsorption on the surface of the SiO_2-CNT

indicates a favorable sorption process. As a heterogeneity parameter, the greater the expected heterogeneity, the smaller the 1/n. The values of $10>n>1$ and $1/n<1$ (Table 3) indicate the favorability of the Hg(II) adsorption on the SiO_2-CNTs (Treybal 1968).

The Temkin Isotherm model considers uniform distribution of the adsorption bonding energies with the adsorbent–adsorbate interactions. The expression is as:

$$q_e = \frac{RT}{b_T}\ln K_T + \frac{RT}{b_T}\ln C_e \tag{11}$$

Where b_T = model constant assigned to the heat of adsorption (J/mole), k_T = Temkin binding energy constant in L/g, R = gas constant (8.314×10^{-3} kJ/mol K), and T = absolute temperature in K.

RT/b_T is considered as the heat of adsorption in J/mol. The plots of q_e versus ln C_e (Fig. 8c) give the values indicate that the heat of sorption is more dominant in a physical adsorption process.

Thermodynamic studies

The related parameters of standard free energy (ΔG^o), enthalpy change (ΔH^o), and entropy change (ΔS^o) were calculated to examine the nature of Hg(II) adsorption on SiO_2-CNT, by linear Van't Hoff expression.

$$\ln K_c = \frac{\Delta S^0}{R} - \frac{\Delta H^0}{RT} \tag{12}$$

The plots of ln K_c versus 1/T (Fig. 9) were used to calculate the ΔH^o and ΔS^o, and the values were listed in Table 4. For the ΔG^o, the following equation was used:

$$\Delta G^0 = \Delta H^0 - T\Delta S^0 \tag{13}$$

where the gas constant R=8.314 J/mol K; T in K; K_c=q_e/C_e (L/mg) the constant of standard thermodynamic equilibrium.

The values of ΔG^o indicate favorable adsorption at higher temperature while the value of ΔH^o (13.3 kJ/mol) indicates the endothermic. The standard entropy (67.5 J/mol K) indicates the strong affinity of SiO_2-CNT toward Hg(II).

Adsorption activation energy

The second-order rate constants (k_2) obtained from the pseudo-second-order kinetic model was used to calculate the

Table 3 Langmuir, Freundlich, and Temkin isotherms constants for Hg(II) adsorption

T (K)	Langmuir isotherm				Freundlich isotherm				Temkin isotherm		
	q_m (mg/g)	k_L (L/mg)	R_L	R^2	1/n	n	k_f (mg/g)	R^2	K_T (L/g)	b_T(KJ/mol)	R^2
296	250	0.14	0.25	0.982	0.67	1.50	34.8	0.992	1.53	0.047	0.987
316	244	0.19	0.39	0.981	0.64	1.57	41.7	0.997	2.03	0.048	0.977
336	227	0.45	0.45	0.878	0.52	1.91	66.7	0.952	5.92	0.057	0.885

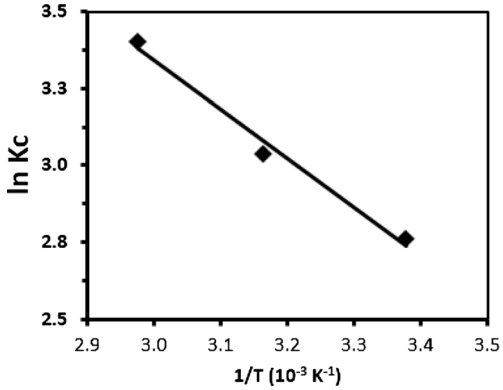

Fig. 9 Plot of ln Kc versus 1/T for Hg(II) adsorption on SiO_2-CNT

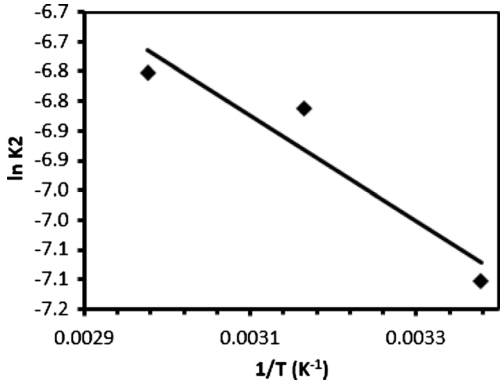

Fig. 10 Plot of ln K_2 versus 1/T (Arrhenius plot) for Hg(II) adsorption on the surface of SiO_2-CNT

adsorption activation energy by applying the Arrhenius equation:

$$\ln k_2 = -\frac{E_a}{R}\left(\frac{1}{T}\right) + constant \quad (14)$$

where R=8.314 J/mol K and E_a = the activation energy in kJ/mol. The physisorption process requires less energy (5–40 kJ/mol) as equilibrium is attained rapidly. The chemisorption mechanism requires large activation energy (40–800 kJ/mol) (Unuabonah et al. 2007).

The experimental data of the effect of contact time at 296, 316, and 336 K were used assuming a pseudo-second-order kinetics. The slopes of the plots of t/q_t against t at 296, 316, and 336 K yield k_2 values. Then, from the Arrhenius plot of ln k_2 against 1/T (Fig. 10), the slope gives the E_a of 12.7 kJ/mol. This assumes the removal process is more dominated by physisorption (nonspecific adsorption) rather chemisorption.

Characterization after adsorption

SEM and EDX were performed to confirm the adsorption of Hg(II) on SiO_2-CNT. The adsorbent samples were collected and dried at 90 °C. Then, EDX spectrum was recorded (Fig. 11). The characteristic peaks of Hg(II) can be observed at 2.195 and 9.987 keV. Also, the carbon peaks at 0.277 keV, oxygen at 0.525 keV, and silica at 1.74 keV can be observed. The presence of the Hg(II) on the adsorbent indicates the affinity of SiO_2-CNT toward mercury.

The morphology of the SiO_2-CNT loaded with Hg(II) was obtained by scanning electron microscope at 20 kV, and the image is depicted in Fig. 11. The distribution of these elements was characterized by EDS mapping. The mercury element species on the surface of the SiO_2-CNT is shown in Fig. 12. The mappings confirm a uniform distribution of silica nanoparticles across the nanotubes and the presence of the mercury on the SiO_2-CNT surface. The mercury elemental map clearly demonstrates that mercury appeared to be uniformly distributed throughout the surface. One possible explanation for this observation is that the mercury diffuses into the SiO_2-CNT and clings to its surfaces.

Table 4 Thermodynamic terms for Hg(II) adsorption

T (K)	ΔG^o (kJ/mol)	ΔH^o (kJ/mol)	ΔS^o (J/mol K)
296	−19.9	13.3	67.5
316	−21.2		
336	−22.7		

Sorption mechanism

Evidence of interactions from EDX, mapping, and other characterization allows us to propose the mechanism as illustrated Fig. 13 to demonstrate the latitude offered by this SiO_2-CNT for mercury removal. The SiO_2-CNT provides a massive of hydroxyl groups as active sites which make it an efficient sorbent for the removal of toxic mercury as proposed in Fig. 13.

Desorption studies (reusability)

The regeneration of the SiO_2-CNT allows its reuse in further cycles and enables recovery of the adsorbed mercury.

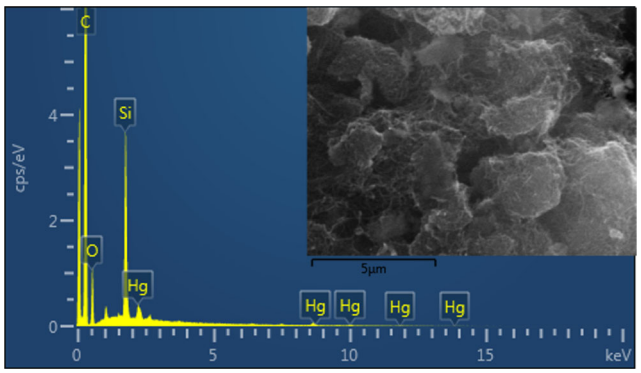

Fig. 11 SEM image with EDX spectrum of mercury-loaded SiO_2-CNT

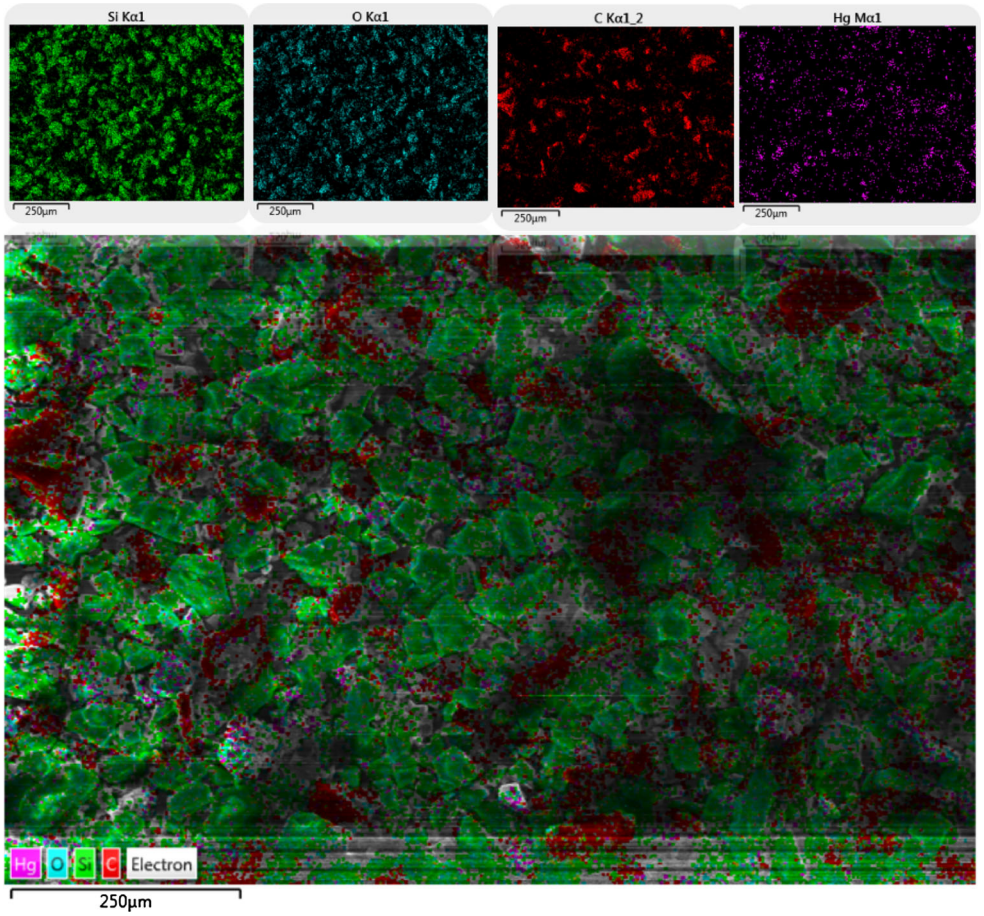

Fig. 12 EDS mapping images of mercury-loaded SiO_2-CNT

The mercury-loaded adsorbent was completely desorbed with 1 M nitric acid. During the repeated adsorption–desorption for five cycles, there was no significant loss in the efficiency of mercury adsorption from their respective solutions. The reusability experiments have proven that the SiO_2-CNT could be regenerated with up to more than 98 % sorption efficiency and reused at least five times in adsorption–desorption cycles.

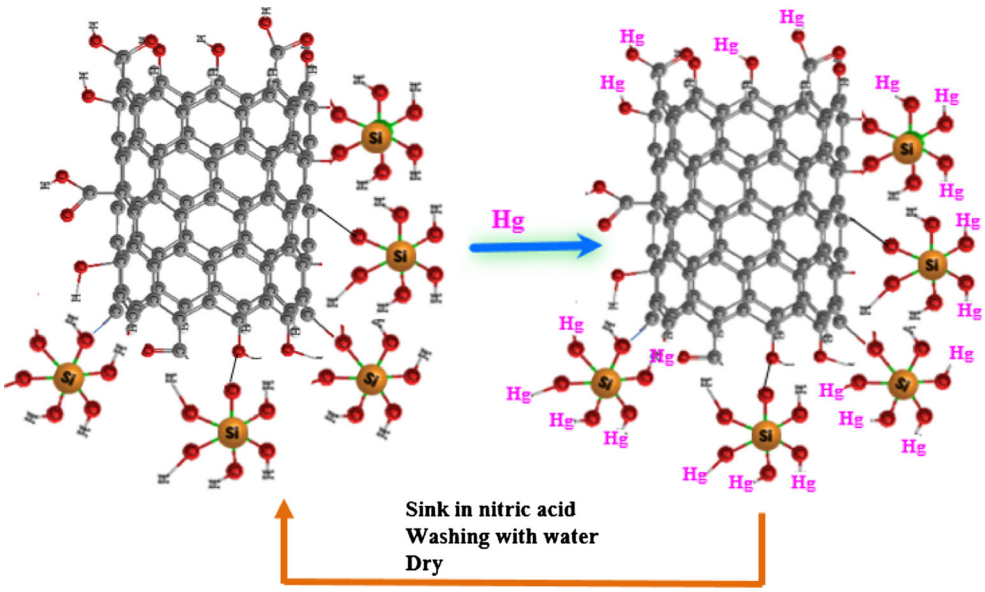

Fig. 13 Schematic illustration of the mechanism of Hg(II) removal by SiO_2-CNT

Wastewater tests

The applicability of the SiO_2-CNT was evaluated using real wastewaters. The aliquots were spiked with 20.0 and 40.0 ppm Hg(II). After that, they were treated with the adsorbent under the obtained optimum conditions. The samples were then analyzed for the mercury. It was found that the removal was almost more than 98 %, indicating the high efficacy and applicability of the adsorbent to be considered as a highly efficient and reusable adsorbent for Hg(II) removal from wastewaters.

Conclusion

This work reported on the utilization of synthesized SiO_2-CNT for the removal of mercury from waters. The efficiency tests were performed in batch mode where the experimental parameters like initial pH, initial concentrations, and contact times were optimized. The optimum pH working range of the reported adsorbent was 4–7. The fastest adsorption rate was within the first 40 min, followed by equilibrium. The results were better fitted to the Freundlich isotherm, rather than Langmuir and Temkin models, with R^2 of 0.99. By the optimization of parameters, the removal percentages of mercury were found to be >98 % in five cycles. The experimental results demonstrate that the SiO_2-CNT is a potential adsorbent, and can be used effectively for the treatment of heavy-metal-ion-containing wastewater.

Acknowledgments The author would like to acknowledge the support provided by the Deanship of Scientific Research (DSR) at King Fahd University of Petroleum & Minerals (KFUPM) for funding this work through project No. JF121009.

References

Anderson DR (1974) In: Lee Smith A (ed) Analysis of Silicones. Wiley-Intersciences, New York, Chapter 10

Anirudhan TS, Divya L, Ramachandran M (2008) Mercury(II) removal from aqueous solutions and wastewaters using a novel cation exchanger derived from coconut coir pith and its recovery. J Hazard Mater 157:620–627

Cui H, Qian Y, Li Q, Zhang Q, Zhai J (2012) Adsorption of aqueous Hg(II) by a polyaniline/attapulgite composite,". Chem Eng J 211–212:216–223

El-Gamel EA, Wortmann L, Arroubb K, Mathur S (2011) SiO2@Fe2O3 core–shell nanoparticles for covalent immobilization and release of sparfloxacin drugw. Chem Commun 47:10076–10078

Freundlich H (1906) Uber die adsorption in losungen (adsorption in solution). Z Phys Chem 57:384–470

Fu X, Feng X, Sommar J, Wang S (2012) A review of studies on atmospheric mercury in China. Sci Total Environ 421–422:73–81

Iijima S (1991) Helical microtubes of graphitic carbon. Nature 354:56–58

Insin N, Tracy JB, Lee H, Zimmer JP, Westervelt RM, Bawendi MG (2008) Incorporation of iron oxide nanoparticles and quantum dots into silica microspheres. ACS Nano 2:197–202

Kadirvelu K, Kavipriya M, Karthika C, Vennilamani N, Pattabhi S (2004) Mercury (II) adsorption by activated carbon made from sago waste. Carbon 42:745–752

Kadirvelu K, Goel J, Rajagopal C (2008) Sorption of lead, mercury and cadmium ions in multi-component system using carbon aerogel as adsorbent. J Hazard Mater 153:502–507

Kim MH, Na HK, Kim YK, Ryoo SR, Cho HS, Lee KE, Jeon H, Ryoo R, Min DH (2011) Facile synthesis of monodispersed mesoporous silica nanoparticles with ultralarge pores and their application in gene delivery. ACS Nano 5:3568–3576

Knocke WR, Hemphill LH (1981) Mercury(II) sorption by waste rubber. Water Res 15:275–282

Labidi NS (2008) Removal of mercury from aqueous solutions by waste brick. Int J Environ Res 2:275–278

Lagergren S (1898) About the theory of so-called adsorption of solution substances, kunglia srenska vertens Ka psakademiens Handlingar. 24: 1–39

Langmuir I (1918) The adsorption of gases on plane surfaces of glass, mica and platinum. J Am Chem Soc 40:1362–1403

Mehdinia A, Akbari M, Baradaran T, Azad M (2015) High-efficient mercury removal from environmental water samples using di-thio grafted on magnetic mesoporous silica nanoparticles. Environ Sci Pollut Res 22:2155–2165

Saifuddin N, Raziah AZ (2007) Removal of heavy metals fromindustrialeffluent using Saccharomyces cerevisiae (Baker's yeast) immobilized in chitosan/lignosulphonate matrix. J Appl Sci Res 3:2091–2099

Saikia BJ, Parthasarathy G (2010) Fourier transform infrared spectroscopic characterization of kaolinite from Assam and Meghalaya, Northeastern India. J Mod Phys 1:206–210

Saleh TA (2011) The influence of treatment temperature on the acidity of MWCNT oxidized by HNO3 or a mixture of HNO3/H2SO4. Appl Surf Sci 257(17):7746–7751

Saleh TA, Gupta VK (2011) Functionalization of tungsten oxide into MWCNT and its application for sunlight-induced degradation of rhodamine B. J Colloid Interface Sci 362(2):337–344

Saleh TA, Gupta VK (2014) Processing methods, characteristics and adsorption behavior of tire derived carbons: a review. Adv Colloid Interf Sci 211:93–101

Sari A, Tuzen M (2009) Removal of mercury(II) from aqueous solution using moss (Drepanocladus revolvens) biomass: Equilibrium, thermodynamic and kinetic studies. J Hazard Mater 171:500–507

Shadbad MJ, Mohebbi A, Soltani A (2011) Mercury(II) removal from aqueous solutions by adsorption on multi-walled carbon nanotubes. Korean J Chem Eng 28:1029–1034

Shawky HA, El-Aassar A, Abo-Zeid DE (2012) Chitosan/carbon nanotube composite beads: Preparation, characterization, and cost evaluation for mercury removal from wastewater of some industrial cities in Egypt. J Appl Polym Sci 125:E93–E101

Treybal RE (1968) Mass Transfer Operations, 2nd edn. McGraw Hill, New York

Unuabonah EI, Adebowale KO, Olu-Owolabi BO (2007) Kinetic and thermodynamic studies of the adsorption of lead (II) ions onto phosphate-modified kaolinite clay. J Hazard Mater 144:386–395

Vasudevan S, Lakshmi J, Sozhan G (2012) Optimization of electrocoagulation process for the simultaneous removal of mercury, lead, and nickel from contaminated water. Environ Sci Pollut Res 19:2734–2744

Wang J, Feng X, Anderson CWN, Xing Y, Shang L (2012) Remediation of mercury contaminated sites—a review. J Hazard Mater 221–222:1–18

Wang Q, Qin W, Chai L, Li Q (2014) Understanding the formation of colloidal mercury in acidic wastewater with high concentration of chloride ions by electrocapillary curves. Environ Sci Pollut Res 21:3866–3872

Webber TN, Chakravarti RK (1974) Pore and solid diffusion models for fixed bed adsorbers. J Am Inst Chem Eng 20:228–238

Yardim MF, Budinova T, Ekinci E, Petrov N, Razvigorova M, Minkova V (2003) Removal of mercury (II) from aqueous solution by activated carbon obtained from furfural. Chemosphere 52:835–841

Yin ZH, Liu X, Su ZX (2010) Novel fabrication of silica nanotubes using multi-walled carbon nanotubes as template. Bull Mater Sci 33:351–355

Yu Y, Addai-Mensah J, Losic D (2012) Functionalized diatom silica microparticles for removal of mercury ions. Sci Technol Adv Mater 13:015008 (11pp)

Zhang M, Wu Y, Feng X, He X, Chen L, Zhang Y (2010) Fabrication of mesoporous silica-coated CNTs and application in size-selective protein separation. J Mater Chem 20:5835–5842

Zhang S, Zhang Y, Liu J, Xu Q, Xiao H, Wang X, Xu H, Zhou J (2013) Thiol modified Fe3O4@SiO2 as a robust, high effective, and recycling magnetic sorbent for mercury removal. Chem Eng J 226:30–38

Zhanga F, Nriagu JO, Itoh H (2005) Mercury removal from water using activated carbons derived from organic sewage sludge. Water Res 39:389–395

Zhu J, Yang J, Deng B (2009) Enhanced mercury ion adsorption by amine-modified activated carbon. J Hazard Mater 166:866–872